Pergamon

PII: S0191-8141(97)00088-6

Journal of Structural Geology, Vol. 20, No. 4, pp. 371 to 384, 1998

0191-8141/98 $19.00 + 0.00

A spatial statistics approach to the quantification of finite strain variation in penetratively deformed thrust sheets: an example from the Sheeprock Thrust Sheet, Sevier Fold-and-Thrust belt, Utah

MALAY MUKUL*

Department of Earth and Environmental Sciences, University of Rochester, Rochester, NY 14627, U.S.A.

(*Received* 11 *December* 1996; *accepted in revised form* 19 *September* 1997)

Abstract—Strain is an important component of the total displacement field in the emplacement of a thrust sheet. The finite strain tensor in a penetratively deformed thrust sheet is a spatial variable. I describe a method for quantitative estimation of the finite strain variation in thrust sheets by applying spatial statistics analysis on strain data collected from a part of the Sheeprock thrust sheet, in the southern Sheeprock Mountains and the West Tintic Mountains, north-central Utah. Strain was measured in the quartzites of the Sheeprock thrust sheet and the spatial statistics method is illustrated using the X/Z strain axial ratios.

The Sheeprock thrust sheet was penetratively deformed during Sevier-age fault propagation folding. I quantified finite strain from quartzites using the modified normalized Fry method and calculated the three-dimensional strain ellipsoid from the quartzites using three orthogonal thin-sections from each oriented field sample. The variation of finite strain in the Sheeprock thrust sheet was best represented by an exponential semivariogram model, which I used to predict values of strain from unsampled locations by ordinary kriging. Cross-validation showed that, in general, the predicted and measured values show good agreement (within 1% of each other). The sampled space was contoured using the measured and predicted strain values to obtain a detailed finite strain variation pattern in a part of the Sheeprock thrust sheet.

INTRODUCTION

Finite strain data are an important part of the data set that must be collected to understand the kinematic history of fold-and-thrust belts. Application of the critically-tapered wedge model (Davis *et al.*, 1983) to the study of the geometry and kinematics of thrust belts (Boyer, 1995) suggests that the magnitude of internal shortening or finite strain in thrust sheets should reflect the geometry and nature of the original sedimentary wedge. If low finite strain values are observed in a thrust sheet, a high initial wedge taper is indicated for the sedimentary prism from which the fold-and-thrust belt evolved (Boyer, 1995; Mitra, 1997). High finite strain values, however, indicate that internal shortening had to occur to build critical wedge taper before thrusts could be emplaced. Basins or portions of basins with higher initial wedge taper produce thrust belts with fewer thrusts having larger individual displacements, lower magnitude of internal shortening, greater width and faster rates of frontal advance (Boyer, 1995).

Finite strain data are also important in the construction of retrodeformable balanced cross-sections (Schwerdtner, 1977; Hossack, 1978, 1979; Woodward *et al.*, 1986; Protzman and Mitra, 1990; Mitra, 1994; McNaught and Mitra, 1996). A complete restoration of any balanced cross-section should involve undoing the total displacement field (Fig. 1). Most restorations, however, only account for the translation and rotation components and ignore the penetrative internal deformation of thrust sheets. This can lead to large errors in restoration, particularly if the thrust sheet was part of a deforming sub-critical sedimentary wedge (Mitra, 1994). The most accurate restorations are obtained by retrodeforming the deformation profile incrementally using the strain history of the thrust sheet as a guide (Groshong *et al.*, 1984; Woodward *et al.*, 1986; McNaught, 1990;

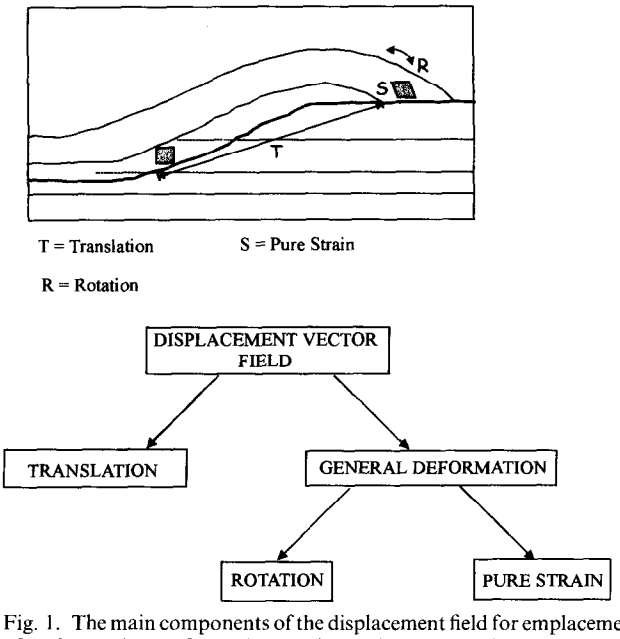

Fig. 1. The main components of the displacement field for emplacement of a thrust sheet [after Mitra (1994)]. The pure strain component is usually not removed in the construction of retrodeformable cross-sections.

*Present address: CSIR Centre for Mathematical Modelling and Computer Simulation, Bangalore 560 037, India.
E-mail: mlym@cmmacs.ernet.in

Evans and Dunne, 1991; Mitra, 1994; McNaught and Mitra, 1996). If incremental strain data are unavailable, inclusion of finite strain data in the restoration process is the next best option.

Once we understand the importance of collection and inclusion of strain data in fold-and-thrust belt studies, we must decide on the best way to collect, organize and use strain data. How strain varies in thrust sheets determines how strain data must be collected and analyzed. For small variations in the distribution of finite strain values within a thrust sheet, finite strain quantification from a few samples from different locations within the sheet would be sufficient; we could use their mean value (along with the standard deviation) as representative for the thrust sheet. However, detailed strain analyses in thrust sheets (Hossack, 1968, 1978; Coward and Kim, 1981; Ramsay *et al.*, 1983; Craddock, 1992; McNaught and Mitra, 1996) have revealed that, in general, there is considerable variation in finite strain values within individual thrust sheets (Mitra, 1994). Thus, there is a need to estimate the spatial variability of strain in a thrust sheet.

Finite strain and strain variation in thrust sheets

In the past, the characteristics of strain and strain variation in thrust sheets across fold-and-thrust belts have been examined in a number of different ways:

(1) The simplest approach is to select one or more samples from each thrust sheet as representative sample(s) and quantify mean strain from them. However, this approach suffers from the basic drawback that the strain values are treated as a batch of numbers, and no account of spatial variability of the data set is made.

(2) A somewhat better approach is one that takes into account spatial variability of the strain data by plotting the magnitude and direction of the long axis of the strain ellipses measured at sample sites (Ramsay *et al.*, 1983). This gives a qualitative estimate of strain variation in the thrust sheet. A further improvement on the method is to contour the sampled space using the plotted values (e.g. Coward and Kim, 1981). With a small data set, we must make simplifying assumptions about the strain variation. For example, assuming strain compatibility (Cutler and Elliott, 1983) and a simple displacement geometry such as inhomogeneous simple shear parallel to the fault, allows two measurements to completely define the pure strain within a thrust sheet (Cutler and Cobbold, 1985). However, most natural thrust systems exhibit complex strain patterns, and the complexity increases from external to internal sheets. Thus, a large data set is required to quantify strain variation within a thrust sheet. The data can be factorized using simple displacement geometries, e.g. the finite strains within the Moine thrust sheet in NW Scotland were factorized into simple shear and longitudinal strain components to examine the variations of these strains (Coward and Kim, 1981). Alternatively, detailed strain data can be collected, and subsequent data analysis may reveal the displacement geometry, e.g. inhomogeneous simple shear (parallel to the fault) in the Helvetic nappes of western Switzerland (Ramsay *et al.*, 1983).

(3) A further improvement on method (2) can be made by actually quantifying not only the strain in the thrust sheet but also its spatial variability. The mathematical function representing the strain variation in thrust sheets could then be used to predict values of strain from anywhere in the sampled area by kriging without making any assumptions about the displacement geometry. The sampled space can then be contoured using the values obtained from kriging analysis. This is the spatial statistics approach presented in this paper. While contouring of the measured strain data can be done using any other interpolation method ranging from simple, qualitative hand contouring to using contouring packages which use more quantitative interpolation algorithms (e.g. Nearest Neighbor Interpolation, Linear Interpolation, Kernel Smoothing and Weighted Fill), it is universally acknowledged that interpolation using kriging is best (e.g. Isaaks and Srivastava, 1989; Cressie, 1993) since kriging has a number of advantages over other interpolation methods. These are as follows:

(i) Smoothing: Kriging smoothes, or regresses, estimates based on the proportion of total sample variance accounted for by random 'noise'. The noisier the data set, the less individual samples represent their immediate vicinity, and the more they are smoothed.

(ii) Declustering: The kriging weight assigned to a sample is lowered to the degree to which its information is duplicated by nearby, highly correlated samples. This helps mitigate the impact of oversampling 'hot spots'.

(iii) Anisotropy: When samples are more highly correlated in a particular direction, kriging weights will be greater for samples in that direction.

(iv) Precision: Given a variogram representative of the area to be estimated, kriging will compute the most precise estimates possible from the available data.

The objective of the spatial statistics method is not merely to create the most accurate contoured plot from measured strain values; the method quantifies strain variation in thrust sheets and uses the results to predict strain values from unsampled locations at any point within the sample area, thereby creating a quantitative data set that can be used in many different ways. For example, the data set can serve as the 'real world' constraint on numerical models of fold-and-thrust belt evolution, or it can be used to develop three-dimensional cross-section balancing techniques particularly for internal parts of fold-and-thrust belts. This aspect of the technique is what makes it more attractive when compared to simpler techniques such as hand contouring or contouring a data set generated using simpler interpolation algorithms. Finite strain data from the

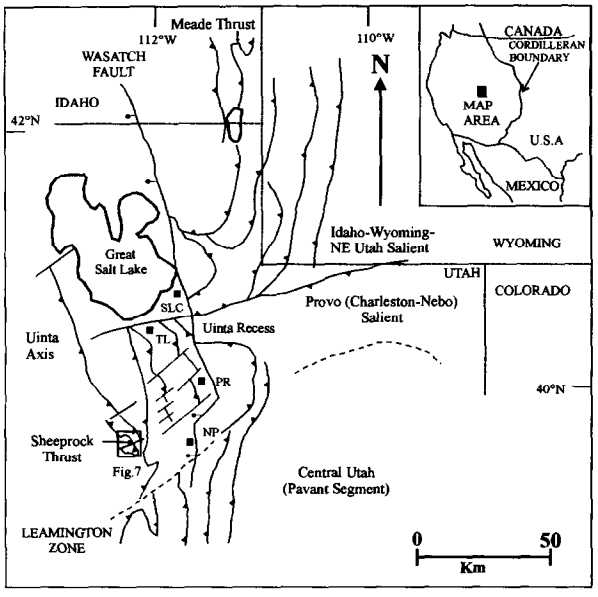

Fig. 2. Simplified map of the Sevier fold-and-thrust belt in Idaho–Wyoming and northern Utah. Three salients separated by transverse zones are shown along with the positions of the major thrusts in the area. Symbols: SLC, Salt Lake City; TL, Tooele; PR, Provo; NP, Nephi.

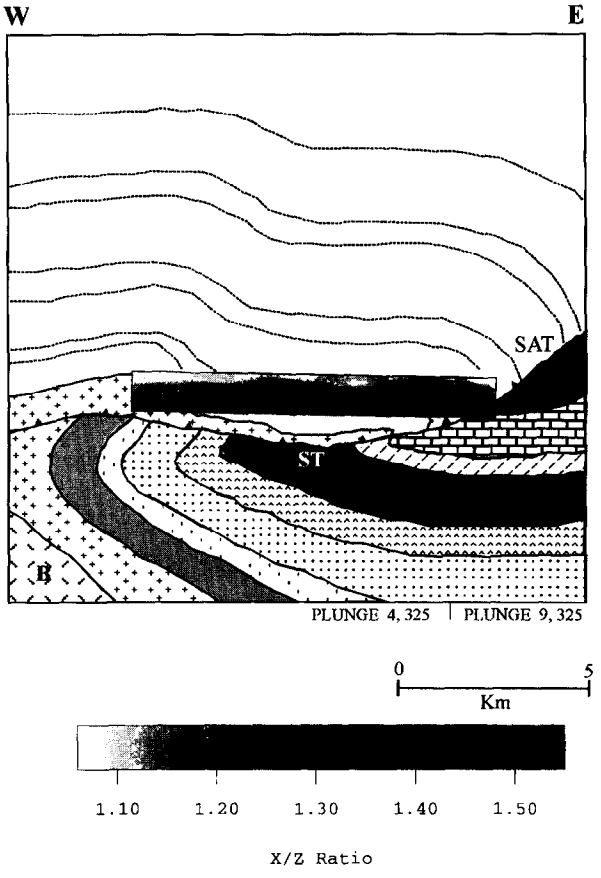

Fig. 3. Composite downplunge projection of the structure of the Sheeprock thrust sheet. The distribution of X/Z axial ratios in downplunge view (along axis 4°, 325°) is also shown (boxed) by an interpolated image diagram. X/Z axial ratios increase from the middle to the base of the sheet near the Sheeprock thrust. A high strain zone is also seen near the hinge of the overturned fault propagation antiform seen in the hanging wall of the Sheeprock thrust. Symbols: B, Basement, ST, Sheeprock thrust, SAT, Sabie Mountain thrust. Patterns used in the figure here are explained in Fig. 5.

Sheeprock thrust sheet are used to illustrate the method. Interpretation of the strain data in the Sheeprock thrust sheet and its implications in cross-section retrodeformation in internal thrust sheets has been published separately in a companion paper (Mukul and Mitra, 1998c). The aim of this paper is to present the spatial statistics method.

The Sheeprock thrust sheet

The Sheeprock thrust sheet is an internal thrust sheet in the Charleston-Nebo (Provo) salient of the Sevier fold-and-thrust belt in north-central Utah (Fig. 2). The geometry of the thrust sheet is dominated by first-order fault propagation folds related to thrusting associated with the Cretaceous Sevier Orogeny (Mukul and Mitra, 1994, 1998a,b, submitted). High-angle breakthrough of the Sheeprock thrust through the fault propagation antiform–synform pair produced a footwall synform. Fault propagation folding in the sheet was followed by fault-bend folding on a ramp in the Sheeprock thrust. Finally, the Sheeprock thrust and the thrust sheet were folded by fault bend folding on a ramp in a younger fault [Midas thrust (?)] (Mukul and Mitra, 1994, submitted; Mitra, 1997). The overall structure of the Sheeprock thrust sheet, as viewed in a down-plunge projection, is shown in Fig. 3. Cleavage observed in the sheet is mostly related to the shortening that produced fault-propagation folding in the sheet and slip along the fault (Mukul and Mitra, 1994). Microstructural analysis in the quartzites indicates that dislocation creep was the dominant deformation mechanism in both the hanging wall (Sussman and Mitra, 1993) and the footwall of the Sheeprock thrust, and the depth of detachment in the internal part of the salient was below the depth of brittle–ductile transition for quartzites (Mukul and Mitra, submitted). Recovery continued in the footwall even after the deformation had ceased (Mukul and Mitra, submitted).

QUANTIFICATION OF FINITE STRAIN FROM THE SHEEPROCK THRUST SHEET

The strain ellipsoid contains three principal sections that define the principal strain ellipses; each can be represented as a vector whose magnitude is the corresponding axial ratio (e.g. the X/Z axial ratio for XZ principal strain ellipse) and whose direction is the orientation of the long axis of the ellipse being considered (Fig. 4). Ideally, the actual magnitudes of the principal axes X, Y and Z of the strain ellipsoid should be used as the magnitudes of three vectors used to represent the strain ellipsoid. However, in geological situations, only axial ratios of ellipses are commonly available.

The Sheeprock thrust sheet is dominated by Proter-

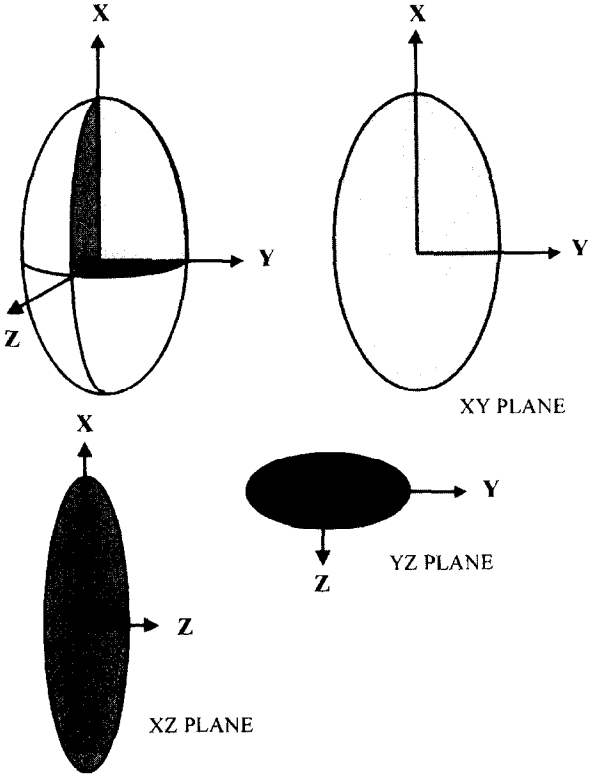

Fig. 4. Geometric representation of the strain tensor by the strain ellipsoid. Three principal sections of the ellipsoid are ellipses; XY, XZ, and YZ planes. The ellipses may be visualized as vectors; the magnitude of the vector is given by the axial ratio between the long and short axes of the ellipse and the direction by the orientation of the long axis.

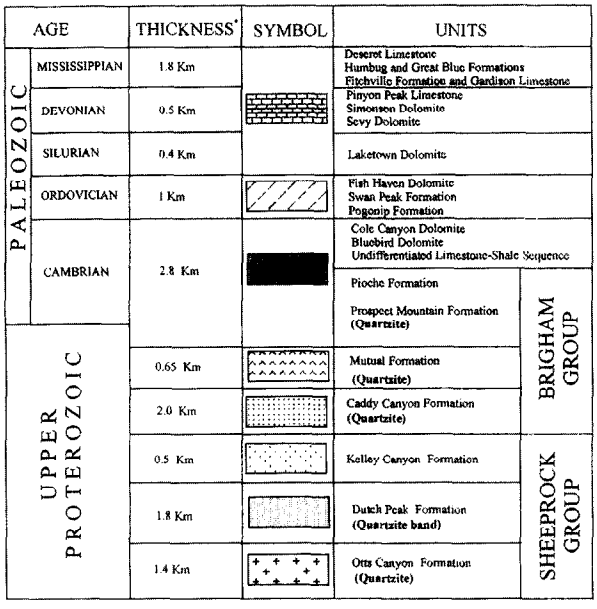

Fig. 5. Composite and simplified stratigraphy of the southern Sheeprock Mountains and the adjacent West Tintic Mountains [after Christie-Blick (1983) and Pampeyan (1989)]. Patterns shown for different stratigraphic units in the figure also serve as the key to patterns used in Figs 3 and 7.

ozoic quartzites (Fig. 5). Finite strain could be measured in these quartzites using the center to center Fry Method (Fry, 1979; Erslev, 1988; Erslev and Ge, 1990; McNaught, 1994) to calculate the three-dimensional strain ellipsoid from quartzite samples.

The center-to-center Fry technique

Fry (1979) developed the Fry method for quantification of strain from aggregates of grains based on the distribution of object centers. Erslev (1988) developed the normalized Fry technique to eliminate effects of two-dimensional grain size on the initial object center distribution, which causes scatter on a Fry plot. Erslev and Ge (1990) developed the INSTRAIN 3.0 program for constructing a normalized Fry plot by approximating each object in an aggregate by a least-squares, best-fit ellipse. McNaught (1994) recognized that the least-squares best-fit ellipse approach (Erslev and Ge, 1990) for approximating grains can run into serious problems when attempting to approximate non-elliptical grains and suggested approximating non-elliptical grains by polygons instead and came up with the modified normalized Fry Method instead. He developed the ANGGRAIN 1.1 program for constructing a normalized Fry plot from co-ordinates of centers of objects and their area using the above approach. McNaught (1994) also suggested the use of an image analyzer to calculate the center and area of objects to make the process more efficient.

Computing the finite strain ellipsoids in the quartzites from the Sheeprock sheet

I used the modified normalized Fry technique (McNaught, 1994) to measure finite strain in the quartzites from the Sheeprock thrust sheet since individual quartz grains in the quartzites are non-elliptical (Fig. 6), and the least-squares best-fit ellipse approach (Erslev, 1988; Erslev and Ge, 1990) would lead to significant errors in grain approximation and calculation of grain centers and area (McNaught, 1990, 1994). The detailed methodology used in computing the finite strain ellipsoids from the quartzites at each sample site in the Sheeprock sheet is described in the Appendix.

THE SPATIAL STATISTICS METHOD

Finite strain values in a thrust sheet are, typically, the end result of a number of processes whose complex interactions cannot be described quantitatively. Although these processes and their interaction are systematic, they are too complex for us to sort out given the present state of our knowledge. As a result, there is uncertainty about how these processes behave between sample locations. In such a situation, where a deterministic approach to understanding the processes is impossible, we may treat the complexity of the processes as apparently random behavior and use probabilistic

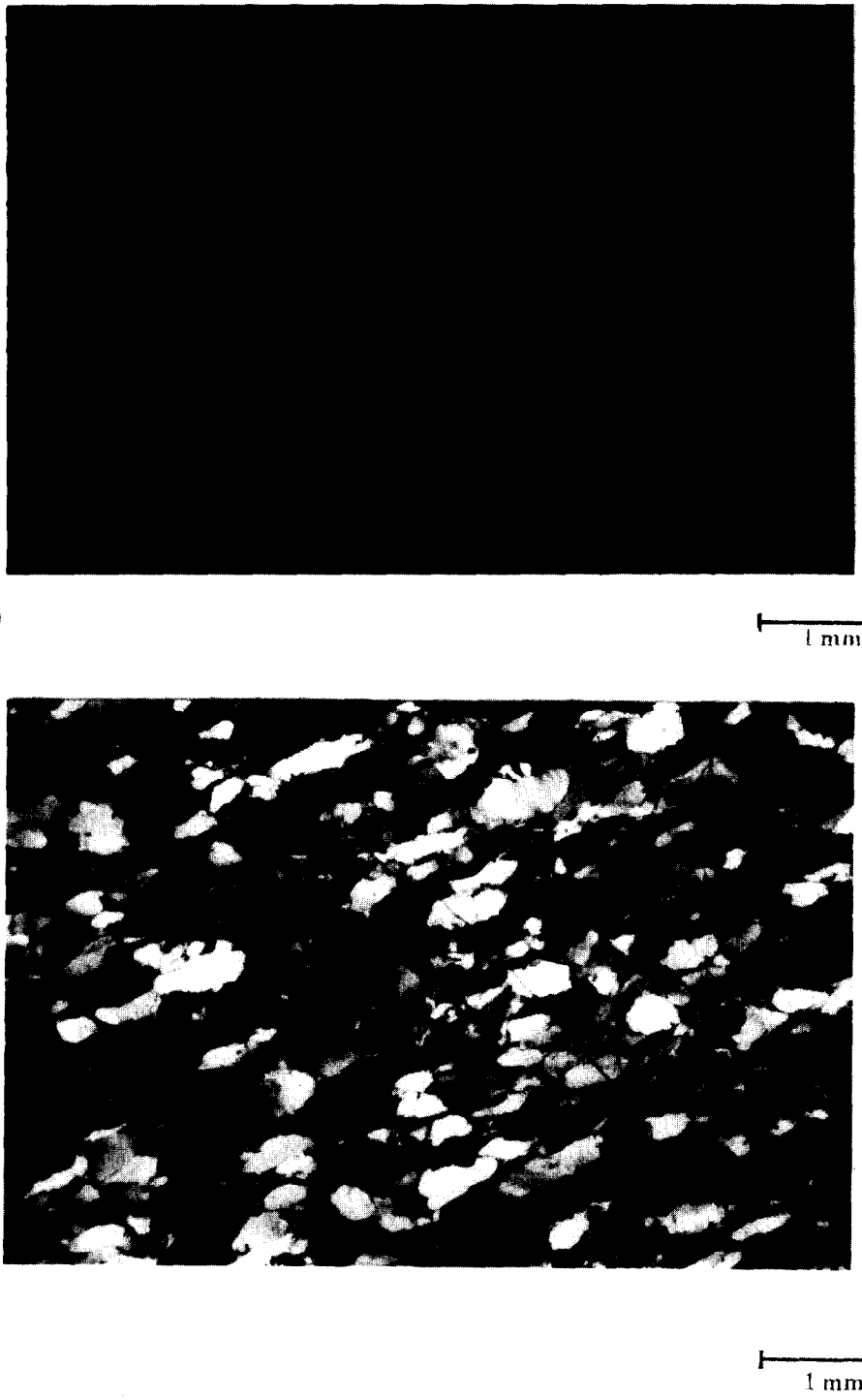

Fig. 6. Black and white tracing of quartz grains (a) from a quartzite sample in the Sheeprock thrust sheet prepared from a photomicrograph of a thin section (b). This drawing is captured by the camera in the JAVA image analysis system. A file containing the grain center and the area of each grain is created which is input into ANNGRAIN (McNaught, 1994).

models that recognize these uncertainties to look at the variation of finite strain in thrust sheets.

The Spatial Model

The General Spatial Model (Cressie, 1993) can be simplified for its application to the problem of studying finite strain variation in thrust sheets. In the most generalized model, I considered the thrust sheet as a three-dimensional space ($\mathbf{R}^3$) and the sampled area in the thrust sheet as index set **D** (which is a fixed subset of $\mathbf{R}^3$ and chosen to contain a three-dimensional regular geometric volume to simplify analytic procedures). The sample locations **s** varied continuously over **D**. However, in natural fold-and-thrust belts, most of the available data are two-dimensional. Exceptions to this are thrust

sheets where subsurface borehole data are abundant, providing the potential for three-dimensional data sets. In the Sheeprock thrust sheet, no borehole data are available, and the strain data are essentially two-dimensional. Therefore, I simplified the generalized model described above for the specific problem of strain in the Sheeprock thrust sheet such that **D** is chosen as a fixed subset of $\mathbf{R}^2$ where $\mathbf{R}^2$ represents either the map (or the horizontal) plane or the down-plunge projection plane; these two cases will be examined separately.

Finite strain in a thrust sheet is likely to be a spatial or a regionalized variable (Matheron, 1963) (i.e. varies in the thrust sheet along and across the strike direction of the associated thrust fault and, therefore, is a variable that is distributed in space) and is neither totally random nor totally deterministic. It is a random variable that exhibits some similarity of values with neighboring locations (in space or time or both, although only space is considered here). While the variation of any of the finite strain axial ratios (X/Y, Y/Z and X/Z) can be studied, the X/Z axial ratio is particularly important as it gives a measure of the maximum shortening in the thrust sheet at a given location. I will illustrate the spatial statistics approach using the X/Z axial ratios measured in the Sheeprock thrust sheet; the variation of axial ratios is quantified and used to predict axial ratios from unsampled points within the sheet.

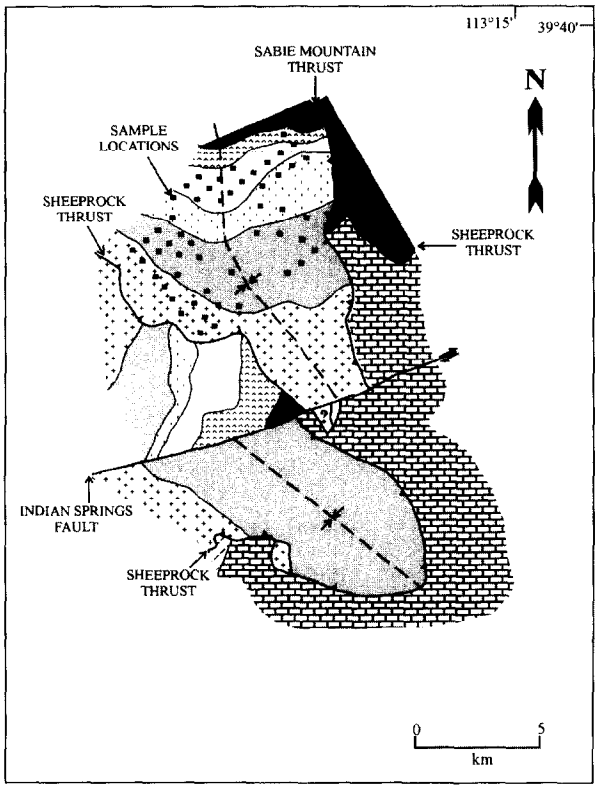

Fig. 7. Location of quartzite samples on the simplified geological map of the southern Sheeprock and the adjacent West Tintic Mountains. Late normal faulting and volcanic rocks have been removed and geology of the thrust sheet interpreted on the basis of field observations.

Sampling quartzites in the Sheeprock thrust sheet

I systematically sampled quartzites on a square grid with spacing of approximately 625 m on the map along and across the strike of the Sheeprock thrust (Fig. 7). Fifty-six samples were collected to fill the grid. The sample sites were also placed away from normal and tear faults in order to avoid cataclasite samples. Systematic sampling on a square grid provides an optimal sampling scheme, which achieves minimum sampling variance (Ripley, 1981); various triangular, rectangular and hexagonal grids would provide other possible optimal schemes. However, the spatial statistics technique does not require that sampling be carried out along a simple grid (Englund and Sparks, 1991; Cressie, 1993) as long as they provide relatively uniform coverage over the sampled area (i.e. the set **D**). The decision to choose the sample locations (i.e. **s**) along some kind of a grid or not depends on the quality of exposure, accessibility or topography. For areas of excellent exposure and accessibility with low relief (such as the Sheeprock thrust sheet), sampling along a grid ensures uniform coverage and optimal data within the sampled area. If the field area does not allow a simple grid of data sampling because of poor exposure, accessibility or unfavorable topography, non-grid data can be collected and used, although care should be taken to minimize gaps and clusters of data as much as possible (Englund and Sparks, 1991).

I chose the size of the sample grid in the Sheeprock thrust sheet to be 625 m (which covered a 5 km × 3 km rectangular area in the Sheeprock thrust sheet) (Fig. 8) so that the number of samples collected from the sheet was optimal; too many samples would make strain quantification very difficult because of the large amount of human time involved in preparing the samples for

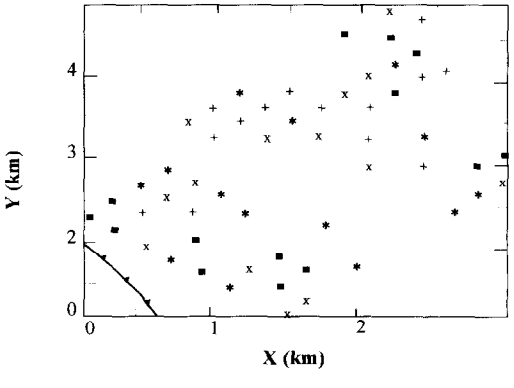

Fig. 8. XY plot of strain (X/Z axial ratios) data from the Sheeprock thrust sheet. The plot gives an idea of the area covered by the sampling and the distribution of the X/Z axial ratios. The approximate position of the west limb of the synformally folded Sheeprock thrust is shown near bottom left of the figure.

quantification of strain, whereas too few samples significantly increase the errors in spatial statistics calculations. For example, a square grid of side 1250 m yielded only about 20 samples from the sheet, and the error between calculated and measured values shot up to 35%. The sample locations are regularly spaced, and, although there are some gaps, a fairly uniform coverage was obtained over the rectangular area (Fig. 8).

Exploratory data analysis (EDA) of X/Z ratios from the Sheeprock thrust sheet

EDA is a standard statistical procedure which is used as the first order of business in any data analysis with the purpose of becoming familiar with the data set. It involves the use of a combination of statistics and graphical displays to look at the range and shape of the frequency distribution, to identify data outliers that may be erroneous or unrepresentative, and to look at the spatial coverage of the data as well as the spatial patterns in the data. EDA, therefore, allows the behavior of the data and its underlying structure to be tested.

In general, highest strain values occur in NW–SE bands along the two edges of the plot, which indicates that high X/Z axial ratios are present close to the thrust (Fig. 8). Low X/Z axial ratios occur away from the thrust near the middle of the Sheeprock thrust sheet. There are no suspect outliers in the data set. The univariate descriptive statistics obtained for the data (Fig. 9) indicate that the data set is nearly symmetrical about its mean since the mean is very close to the median and approximately halfway between the minimum and maximum values. However, the coefficient of skewness (0.6874) indicates a slight positive skewness for the distribution. The kurtosis value (4.8335) indicates a slightly leptokurtic or slightly more peaked distribution than a normal distribution. Thus, the distribution of X/Z axial ratios in the Sheeprock thrust sheet is close to a normal distribution. The deviations from a normal distribution could be caused by the presence of outliers and/or lack of sufficient number of samples. One way to test this is to construct a probability plot (Fig. 9): a cumulative frequency plot scaled so that a normal distribution plots as a straight line. The probability plot for the X/Z axial ratios in the Sheeprock thrust sheet (Fig. 9) indicates that the distribution approximates a normal population. Outliers are, however, present near both the high and low X/Z axial ratios. The nature of the distribution (whether a distribution is normal, log–normal, binomial, etc.) does not affect the way in which the spatial statistics analysis is carried out, except that for highly skewed distributions such as the log–normal distribution, it is more useful to use the spatial statistics method on log-transformed data. Since the distribution for the X/Z axial ratios in the Sheeprock thrust sheet approximates a normal population, no transformations on the data are required. The outliers were retained in the data set to investigate the amount of error introduced in the analysis when all 56 samples used to estimate X/Z axial ratios in the Sheeprock thrust sheet are considered valid samples.

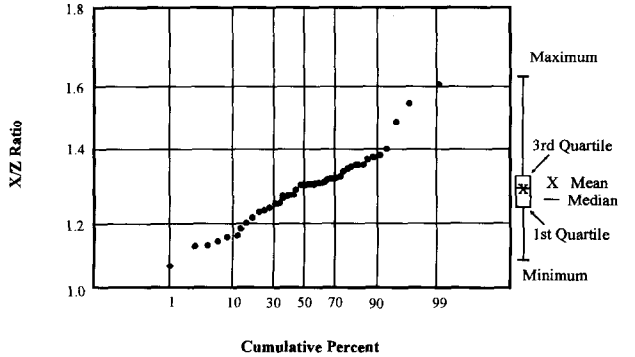

Fig. 9. Probability plot of finite strain (X/Z axial ratios) data from the Sheeprock thrust sheet. The plot shows that the X/Z axial ratios approximate a normal population. Univariate descriptive statistics for the data indicates a positively skewed, slightly leptokurtic distribution.

Variogram analysis of X/Z axial ratios in the Sheeprock thrust sheet

A variogram is defined as a plot of the variance (one-half the mean squared difference) of paired sample measurements as a function of the distance and direction between samples. Typically, all possible sample pairs in a given direction are examined, and grouped into classes (lags) of approximately equal distance. Variograms provide a method of quantifying the commonly observed relationship that samples close together will tend to have more similar values than samples far apart. The computation, interpretation and modeling of variograms is an evaluation of the spatial correlation structure of the sample data set. Assuming that a X/Z axial ratio measurement at any point in the thrust sheet represents nearby locations better than locations farther away, variogram analysis helps us decide how well a measurement represents another location a specific distance and direction away. Variogram analysis is the key to the spatial statistics method and kriging; it is the most important step in creating the comprehensive, quantitative data set that this analysis aims to create.

For the purpose of variogram analysis, I considered the measured X/Z axial ratios to be represented by the probabilistic function $Z(s_i)$, s_i being the sample locations. I next evaluated the relationship between the value of Z at any given point and the value of the other $n-1$ points ($n=56$ here). Given that the difference in values of Z between any two points depends only on the distance between them and their relative orientation (i.e. the separation vector **h**), the semivariogram is defined by the following formula (Cressie, 1993):

$$\gamma(h) = \frac{1}{2N(h)} \sum_{i=1}^{N(h)} [Z(S_i + h) - Z(S_i)]^2, \qquad (1)$$

where N is the number of pairs (separated by the distance $|h|$) considered. Semivariograms plot the variance of pairs of measurements against the distances separating the pairs. If measurements at all possible sample locations within the thrust sheet were available, the variance of all pairs of measurements that satisfy each combination of distance and direction could be computed and the true variogram for a site obtained. In practice, however, it is not possible to have measurements at all locations and, with limited data, only a subset of the true variogram can be obtained. This is termed the experimental semivariogram. The variance for groups of pairs of measurements in class intervals of similar distance and direction was computed. A graph of variances vs distance for a particular direction was plotted, and a model curve was fitted to the graph (Fig. 10); the model is then an approximation of the true variogram.

Experimental semivariograms constructed to display spatial variation of a variable in a given direction are termed 'directional semivariograms'. In constructing a directional semivariogram, a tolerance is usually set on the magnitude and the direction of the separation vector

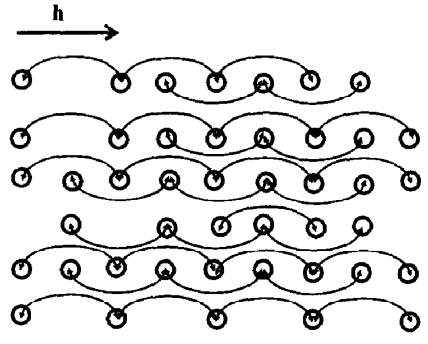

(A)

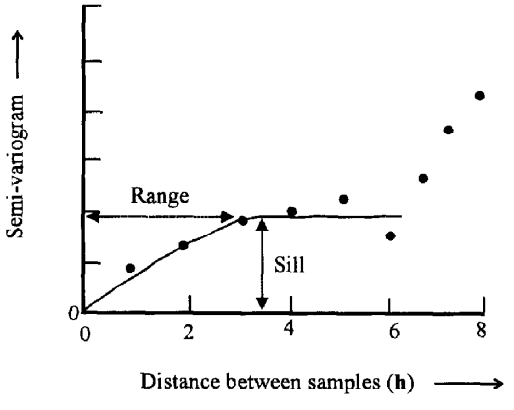

(B)

Fig. 10. Construction of a direction semivariogram. Pairs considered for variogram calculation for $\mathbf{h} = 2$ and E–W orientation is shown in (a). Variogram model fit to semivariogram values calculated for different values of $\mathbf{h}$ is shown in (b). Circles represent sample sites.

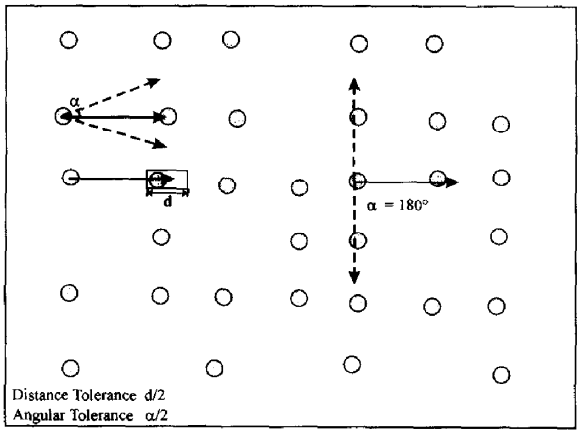

Fig. 11. Definition of the distance and angular tolerances for the separation vector **h**. The distance tolerance is defined as the tolerance on the length of the separation vector and the angular tolerance is the tolerance on the orientation of the separation vector. Calculation of a variogram with an angular tolerance of 90° (or $a = 180°$) is equivalent to averaging variograms calculated in all directions; the omnidirectional semivariogram. Circles represent sample sites.

h (Fig. 11). This ensures that slight variations in distance and orientation between sample locations do not affect the semivariogram computing process. When sample stations are irregularly spaced, setting a tolerance limit on **h** becomes essential.

Calculating a variogram with an angular tolerance of 90° is equivalent to averaging variograms calculated in all directions, and is referred to as an *omnidirectional semivariogram*. The angular tolerance of 90° on either side of any specified direction line allows all pairs to be included in the computation of the semivariogram regardless of direction. This maximizes the number of pairs in each distance class and gives the smoothest or best experimental variogram. Therefore, semivariogram models fitted to the omnidirectional experimental semivariogram give the best estimate of model parameters for the semivariogram model. For the X/Z axial ratios in the Sheeprock thrust sheet, the omnidirectional semivariogram is shown in Fig. 12(a). Once an initial estimate of the omnidirectional semivariogram model is obtained, the model must next be tested to see how it fits directional experimental semivariograms.

I applied this procedure to the Sheeprock strain data (Fig. 12a) and examined linear, spherical, exponential, power and Gaussian semivariogram models. On visual examination, the exponential model seemed to fit the omnidirectional and directional experimental semivariograms the best. To double check this, I carried out the entire spatial statistics analysis using each of the semivariogram models and compared the errors obtained between the measured and predicted models. The exponential model (Fig. 12b) gave the best results. This confirmed the initial observation that the best fit on the omnidirectional experimental semivariogram for the X/Z axial ratios in the Sheeprock thrust sheet was given

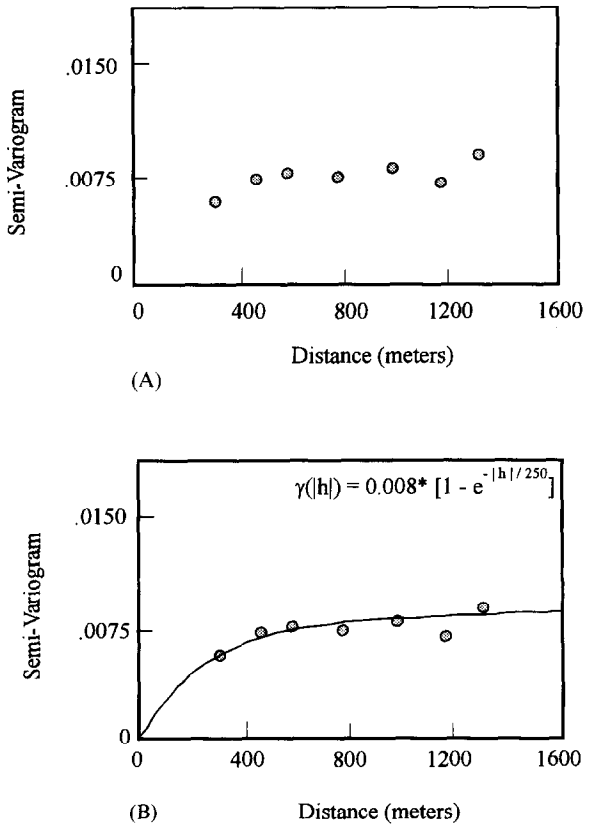

Fig. 12. Omnidirectional semivariogram for X/Z axial ratios in the Sheeprock thrust sheet. The experimental semivariogram is shown in (A) and the variogram model fit in (B). The exponential model (sill 0.008 and range 750 m) gives the best fit on the experimental semivariogram.

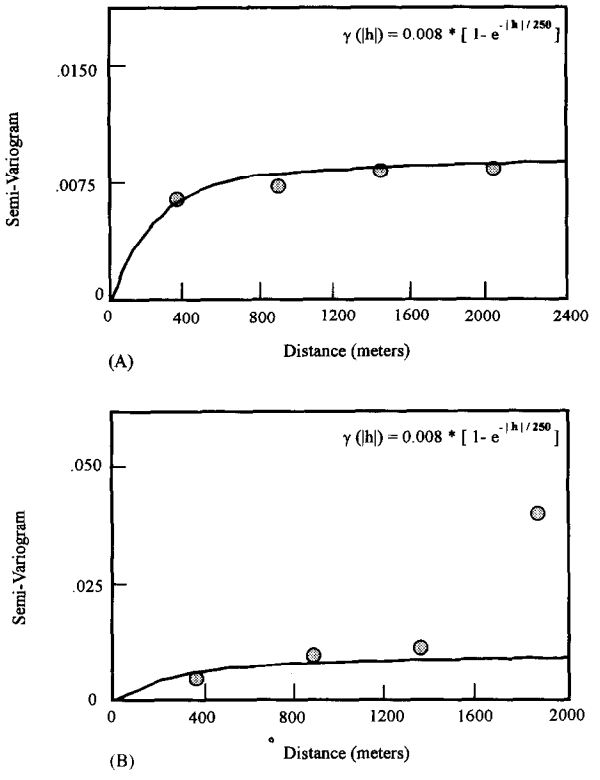

Fig. 13. Directional semivariogram for X/Z axial ratios in the Sheeprock thrust sheet. Semivariograms parallel and perpendicular to the transport direction are shown in (A) and (B), respectively. The exponential model (sill 0.008 and range 750 m) used to fit the omnidirectional semivariogram gives good fit on the directional semivariograms.

by the exponential model defined by the following equation:

$$\gamma(|h|) = c[1 - e^{\frac{-3|h|}{a}}] \quad (2)$$

where c is the positive variance contribution or sill value, and a is the practical range, i.e. the distance at which the semivariogram value is 95% of the sill. This model reaches its sill asymptotically and has a linear behavior at the origin. The omnidirectional semivariogram for the X/Z axial ratios in the Sheeprock thrust sheet is an exponential model where $c = 0.008$ and $a = 750$ m and can be written as:

$$\gamma(|h|) = 0.008[1 - e^{\frac{-|h|}{250}}]. \quad (3)$$

The directional variograms along and across the transport direction of a thrust sheet are most important in finite strain studies in thrust sheets. Thus, the omnidirectional semivariogram model defined above must fit the two directional variograms for it to be a valid model. Good fits are obtained when the exponential omnidirectional semivariogram is superimposed on the transport parallel and transport perpendicular semivariograms (Fig. 13). Thus, the exponential model (equation (3)) describes the variation of finite strain (XZ axial ratios) in the Sheeprock thrust sheet in plan. It is important to note at this point that a semivariogram must be calculated anew for each data set as the variogram model is a custom fit to the data set. This spatial model can be now used to predict XZ axial ratios from unsampled points within the sample area by kriging.

Spatial prediction and kriging

I used a probabilistic model to quantify the strain variation within a thrust sheet by constructing semivariograms. In this model, the available sample data were viewed as the result of some probabilistic process. This conceptualization is a useful one for the problem of estimating values at unknown locations. It not only allows us to make predictions about how apparently random processes behave where we have not sampled them but also gives us some ability to gauge the accuracy of the estimates and assign confidence intervals to them. In practice, we will use a probability model and define the best possible estimator and use it to carry out point estimations of finite strain values from any point in the Sheeprock thrust sheet.

Spatial estimator

Ordinary kriging has been described as the 'best linear unbiased estimator (BLUE)' (Isaaks and Srivastava,

1989) for point estimations. Ordinary kriging is 'linear' because its estimates are weighted linear combinations of the sampled data. It is 'unbiased' because it tries to reduce the mean residual or error to 0. It is 'best' because it aims at minimizing the variance of the errors.

Since we are not working with a data set that includes all possible strain measurements from the Sheeprock thrust sheet, the true mean error and the error variance of the data are unknown. The best that we can do in this situation is to build a probabilistic model of the data and work with the average error and the error variance for the model. For ordinary kriging, we use a model in which bias and the error variance can both be calculated, and then choose weights for the nearby samples that ensure that the average error for the model is exactly 0 and the modeled error variance is minimized.

Since ordinary kriging is a linear estimator, at every point where we do not have a sample, we will estimate the unknown true value using a weighted linear combination of the available samples:

$$Z^* = \sum_{i=1}^{n} \lambda_i Z_i, \tag{4}$$

where n is the number of samples (or known values of the finite strain variable). For the estimates to be unbiased, the weights must add to 1 (Isaaks and Srivastava, 1989):

$$\sum_{i=1}^{n} \lambda_i = 1. \tag{5}$$

Assuming an unbiased estimator, the error variance, σ^2, of a set of k estimates can be written as:

$$\sigma^2 = \frac{1}{k} \sum_{i=1}^{k} [Z_i - Z_i^*]^2, \tag{6}$$

where Z_i and Z_i^* are actual and estimated finite strain values at k estimation points. Once again, since the actual values are unknown, we turn to probabilistic models and define the variance of modeled error instead. Minimizing the modeled error variance leads to the following ordinary kriging equation (Isaaks and Srivastava, 1989):

$$\sum_{j=1}^{n} \lambda_j \gamma_{ij} - \mu = \gamma_{i0} i = 1, \ldots, n \tag{7}$$

where μ is a Lagrange parameter, γ_{ij} is the variogram model between two known points i and j, whereas γ_{i0} is the variogram model between a known point i and the location to be estimated. In matrix form

$$\gamma_{if} \lambda = \gamma_{i0} \tag{8}$$

and the solution is

$$\lambda = \gamma_{if}^{-1} \gamma_{i0} \tag{9}$$

where

$$\lambda = \begin{bmatrix} \lambda_1 \\ . \\ . \\ \lambda_n \\ -\mu \end{bmatrix} \gamma_{if} = \begin{bmatrix} \gamma_{11} & . & . & \gamma_{1n} & 1 \\ . & . & . & . & . \\ . & . & . & . & . \\ \gamma_{n1} & . & . & \gamma_{nn} & 1 \\ 1 & . & . & 1 & 0 \end{bmatrix} \gamma_{i0} = \begin{bmatrix} \gamma_{10} \\ . \\ . \\ \gamma_{n0} \\ 1 \end{bmatrix}$$

I analyzed finite strain data (X/Z axial ratios) from the Sheeprock using this approach and then prepared a contoured map of the X/Z axial ratios (Fig. 14a) from the results obtained by ordinary kriging using the GEO-EAS 1.2.1 software. An interpolated image map was also prepared (Fig. 14b). However, at this stage, we also need to know how well the estimation works. This can be achieved by cross-validation, which involves estimating values at each sampled location in an area by kriging with the neighboring sample values (excluding the value of the point being estimated). X/Z axial ratios were estimated in this way at each of the 56 sample locations in the Sheeprock thrust sheet. The estimates were compared with the measured values in order to calculate the error in estimation. Errors between the estimated and measured values were evaluated at different positions in the distribution (Table 1). Errors increased at the minimum and maximum ends of the distribution of X/Z axial ratios. This is to be expected because the distribution deviates from a normal distribution near the minimum and maximum values (Fig. 9). Estimation errors for the rest of the distribution are approximately within 1% (Table 1). Thus, the variogram model used to quantify the finite strain variation in the Sheeprock thrust sheet is a reasonably accurate one. Ordinary kriging performed using the variogram model also results in fairly accurate estimations of the X/Z axial ratios from unsampled points in the thrust sheet. However, this also raises an important question; how would anomalous values (e.g. from fault zones) affect the data analysis? The key to dealing with an anomalous value in the analysis would be to determine whether the value is part of the population being analyzed or part of a different population. EDA would be helpful in identifying this. If the anomalous value is part of a different population, we should expect large errors in the predicted strain values in the vicinity of the anomalous value; this statement can be substantiated by the high errors seen at the minimum and maximum ends of the distribution of X/Z ratios (Table 1) where deviation from the normal population is most evident. The best way to deal with the situation would be to remove the anomalous values from the data set and analyze each population separately (e.g. treat strain in a fault zone as a separate population from the rest of the thrust sheet).

Results from the analysis (Fig. 14) indicate that, in plan view, finite strain (X/Z axial ratios) decreases away from the Sheeprock thrust. An increase in the X/Z axial ratios is also observed along the strike of the fault from NW to SE. Studies of kinematics of fold and thrust belts involve construction of retrodeformable balanced cross-sections.

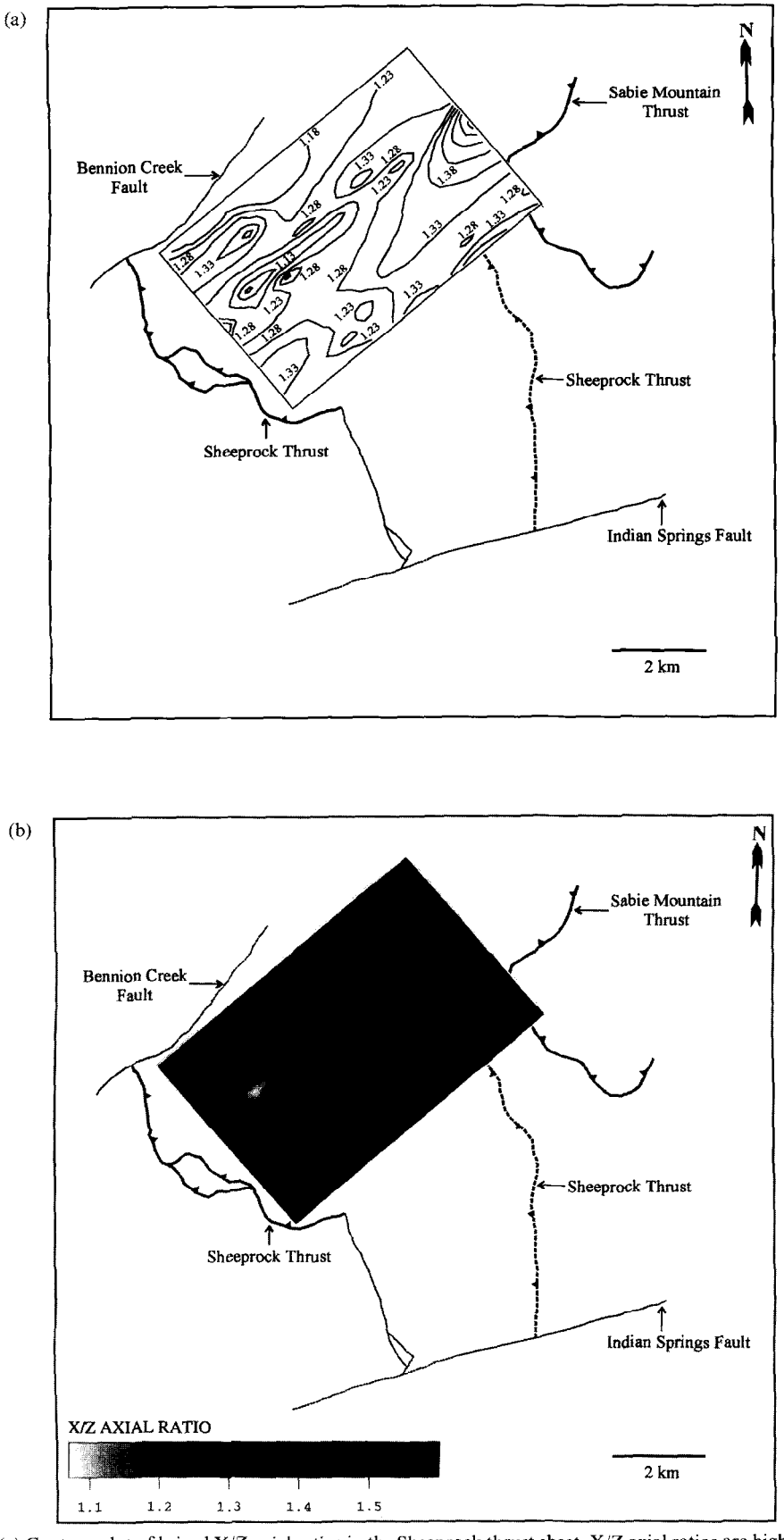

Fig. 14. (a) Contour plot of kriged X/Z axial ratios in the Sheeprock thrust sheet. X/Z axial ratios are higher near the thrust and decrease towards the center of the thrust sheet. (b) Interpolated image map of the kriged X/Z axial ratios in the Sheeprock thrust sheet. Higher strains are seen near the Sheeprock thrust. Strain also increases along strike of the Sheeprock thrust from NW to SE. Least strain is observed near the center of the thrust sheet. The west limb of the folded Sheeprock thrust strikes approximately NW–SE.

Table 1. Error analysis

	Measured	Estimated	Error %
Minimum	1.067	1.160	8.72
25th percentile	1.225	1.238	1.06
Median	1.284	1.273	0.86
Mean	1.283	1.278	0.39
75th percentile	1.319	1.140	1.14
Maximum	1.604	1.429	10.90

Thus, the nature of strain variation in the transport or the down-plunge projection plane is important. The spatial statistics method was applied to samples in the hanging wall of the Sheeprock thrust sheet (Fig. 3) to investigate the applicability of the method to cross-sectional data. First, the sample locations in the map (Fig. 7) were projected along the axis 4°, 325° and plotted on the down-plunge projection of the structure of the Sheeprock thrust sheet. Next, the three-dimensional strain ellipsoids calculated at each of the sample locations were projected along the axis 4°, 325° using the algorithm described by Gendzwill and Stauffer (1981). The axial ratios of the projected ellipses were used at each sample location in the down-plunge projection. An exponential model was once again used to model the strain variation in the sheet. An interpolated image diagram was constructed from the kriged data (Fig. 3).

The interpolated image diagram (Fig. 3) documents a decrease in strain as we move away from the thrust higher up into the thrust sheet. This trend has been recorded in thrust sheets worldwide (Hossack, 1968, 1978; Coward and Kim, 1981; Ramsay *et al.*, 1983; Mitra, 1994). There is also a high-strain region seen near the hinge of the fault propagation antiform in the hanging wall of the Sheeprock thrust. A detailed discussion of the strain patterns in the Sheeprock thrust sheet produced by the method and its geological implications are discussed in the companion paper in this volume (Mukul and Mitra, 1998c).

DISCUSSION

Quantification of strain variation and estimation of finite strain from unsampled points in a thrust sheet by kriging facilitates the use of strain and strain variation data for a number of possible applications. It improves the accuracy of retrodeformable balanced cross-sections by providing a detailed and improved description of strain and strain variation in thrust sheets to account for the pure strain component of the total displacement field. It also facilitates the use of strain and strain variation data in modeling natural structures. The spatial statistics algorithm looks at the overall strain variation in a thrust sheet without considering individual factors that cause the variation. Strain variation in a thrust sheet is caused by a complex interplay of variations in lithology, grain-size, deformation mechanisms, pressure, temperature, stress and strain rate. It is not possible to isolate the variations caused by each of these factors. The spatial statistics approach allows us to overcome the complexity of the system by defining a probabilistic model using the measured strain values. This approach is a valid way of simplifying the problem.

The results obtained from this approach will also serve as a cross-check on results obtained from independent numerical models of evolution of fold and thrust belts. Valid numerical models must approximate the strain variation patterns obtained from the spatial statistics approach. Strain variation functions obtained using spatial statistics can be included in the numerical modeling process. For example, the semi-variogram model can be used as the interpolation function in a finite element numerical model for the deformation in the sheet.

The spatial statistics approach, therefore, offers a systematic method for studying strain variation in penetratively deformed thrust sheets. The main strength of the method lies in the fact that it can quantify strain variation in thrust sheets and predict strain at unsampled points within the sampled region in the thrust sheet.

Acknowledgements—This paper is an outgrowth of a doctoral dissertation done at the University of Rochester. This work was supported by NSF grant EAR-9418688 to G. Mitra and by grants from the American Association of Petroleum Geologists (Peter W. Gester Memorial Grant), the Geological Society of America, and Sigma Xi to M. Mukul. Reviews by G. Mitra, Mark Evans, and an anonymous reviewer helped strengthen the paper. GEO-EAS 1.2.1 was used for the spatial statistics analysis carried out in this paper.

REFERENCES

Boyer, S. E. (1995) Sedimentary basin taper as a factor controlling the geometry and advance of thrust belts. *American Journal of Science* **295**, 1220–1254.

Christie-Blick, N. H. (1983) Structural geology of the southern Sheeprock Mountains, Utah: Regional significance. In *Techtonic and stratigraphic studies in the Eastern Great basin*. Eds D. M. Miller, V. R. Todd and K. R. Howard. Geological Society of America Memoir **157**, 101–124.

Coward, M. P. and Kim, J. H. (1981) Strain within thrust sheets. In *Thrust and Nappe Tectonics*, eds K. R. McClay and N. J. Price. Special Publications: Geological Society of London **9**, 275–292.

Craddock, J. P. (1992) Transpression during tectonic evolution of the Idaho–Wyoming fold-and-thrust belt. In *Regional Geology of Eastern Idaho and Western Wyoming*, eds P. K. Link, M. A. Kuntz and L. B. Platt. Geological Society of America Memoir, **179**, 125–139.

Cressie, N. (1993) *Statistics for Spatial Data*. John Wiley and Sons, New York.

Cutler, J. M. and Cobbold, P. R. (1985) A geometric approach to two-dimensional finite strain compatibility: interpretation and review. *Journal of Structural Geology* **7**, 727–735.

Cutler, J. M. and Elliott, D. (1983) The compatibility equations and the pole to the Mohr circle. *Journal of Structural Geology* **5**, 287–297.

Davis, D., Suppe, J. and Dahlen, F. A. (1983) Mechanics of fold and thrust belts and accretionary wedges. *Journal of Geophysical Research* **88** (B2), 1153–1172.

DePaor, D. G. (1990) Determination of the strain ellipsoid from sectional data. *Journal of Structural Geology* **12**, 131–137.

Englund, E. and Sparks, A. (1991) *GEO-EAS 1.2.1 Geostatistical Environmental Assessment Software*. Environmental Monitoring Systems Laboratory, Office of Research and Development, U.S. Environmental Protection Agency, Las Vegas.

Erslev, E. A. (1988) Normalized center-to-center strain analysis of packed aggregates. *Journal of Structural Geology* **10**, 201–209.
Erslev, E. A. and Ge, H. (1990) Least-squares center-to-center and mean object ellipse fabric analysis. *Journal of Structural Geology* **12**, 1047–1059.
Evans, M. A. and Dunne, W. M. (1991) Strain factorization and partitioning in the North Mountain thrust sheet, central Appalachians: U.S.A. *Journal of Structural Geology* **13**, 21–36.
Fry, N. (1979) Random point distribution and strain measurement in rock. *Tectonophysics* **60**, 89–105.
Gendzwill, D. J. and Stauffer, M. R. (1981) Analysis of triaxial ellipsoids: their shapes, plane sections, and plane projections. *Mathematical Geology* **13**, 135–152.
Groshong, R. H., Pfiffner, O. A. and Pringle, L. R. (1984) Strain partitioning in the Helvetic thrust belt of eastern Switzerland from the leading edge to the internal zone. *Journal of Structural Geology* **6**, 5–18.
Hossack, J. R. (1968) Pebble deformation and thrusting in the Bygdin area (Southern Norway). *Tectonophysics* **5**, 315–339.
Hossack, J. R. (1978) The correction of stratigraphic section for tectonic finite strain in the Bygdin area, Norway. *Journal of Geological Society of London* **135**, 229–241.
Hossack, J. R. (1979) The use of balanced cross-sections in the calculation of orogenic contraction: a review. *Journal of Geological Society of London* **136**, 705–711.
Isaaks, E. H. and Srivastava, R. M. (1989) *An Introduction to Applied Geostatistics*. Oxford University Press, New York.
McNaught, M. A. (1990) The use of retrodeformable cross-sections to constrain the geometry and interpret the deformation of the Meade thrust sheet, southeastern Idaho and northern Utah. Ph.D. dissertation, University of Rochester.
McNaught, M. A. (1994) Modifying the normalized Fry method for aggregates of non-elliptical grains. *Journal of Structural Geology* **16**, 493–503.
McNaught, M. A. and Mitra, G. (1996) The use of finite strain data in constructing a retrodeformable cross-section of the Meade thrust sheet, southeastern Idaho. *Journal of Structural Geology* **18**, 573–583.
Matheron, G. (1963) Principles of geostatistics. *Economic Geology* **58**, 1246–1266.
Milton, N. J. (1980) Determination of the strain ellipsoid from measurements on any three sections. *Tectonophysics* **64**, T19–T27.
Mitra, G. (1994) Strain variation in thrust sheets of the Sevier fold-and-thrust belt, Idaho–Utah–Wyoming: Implications for section restoration and wedge taper evolution. *Journal of Structural Geology* **16**, 585–602.
Mitra, G. (1997) Evolution of salients in a fold-and-thrust belt: the effects of sedimentary basin geometry, strain distribution and critical taper. In *Evolution of Geologic Structures from Macro-to Micro-scales*, ed. S. Sengupta. Chapman and Hall, London (in press).
Mukul, M. and Mitra, G. (1994) Deformation history of the Sheeprock thrust sheet: new interpretations based on structural analysis. *Geological Society of America Abstracts with Programs* **26**, 49.
Mukul, M. and Mitra, G. (1998a) Controversies in the geology of the Sheeprock thrust sheet, Sevier fold-and-thrust belt, Utah—A re-examination based on new evidence. In *Geology of the Sheeprock Thrust Sheet, Utah—New Insights*. Utah Geological Survey Miscellaneous Publication **98–1**, Chapter 1, 56 pp.
Mukul, M. and Mitra, G. (1998b) Stratigraphy and structural geology of the southern Sheeprock and the adjacent West Tintic Mountains, Utah—A review and new interpretations based on structural analysis. In *Geology of the Sheeprock Thrust Sheet, Utah—New Insights*. Utah Geological Survey Miscellaneous Publication **98–1** Chapter 2, 56 pp.
Mukul, M. and Mitra, G. (1998c) Finite strain and strain variation analysis in the Sheeprock thrust sheet: an internal thrust sheet in the Provo salient of the Sevier fold-and-thrust belt, Central Utah. *Journal of Structural Geology* **20**, 385–405.
Pampeyan, E. H. (1989) Geological map of the Lynndyl 30- by 60-minute Quadrangle, west-central Utah. United States Geological Survey Miscellaneous Investigations Map I-1830, scale 1:24,000.
Protzman, G. M. and Mitra, G. (1990) Strain fabrics associated with the Meade thrust: implications for cross-section balancing. *Journal of Structural Geology* **12**, 403–417.
Ramsay, J. G., Casey, M. and Kligfield, R. (1983) Role of shear in development of the Helvetic fold-thrust belt of Switzerland. *Geology* **11**, 439–442.
Ripley, B. D. (1981) *Spatial Statistics*. Wiley, New York.
Schwerdtner, W. M. (1977) Geometric interpretation of regional strain analysis. *Tectonophysics* **39**, 515 531.
Shimamoto, T. and Ikeda, Y. (1976) A simple algebraic method for strain estimation from deformed ellipsoidal objects—1. Basic theory. *Tectonophysics* **36**, 315–337.
Sussman, A. J. and Mitra, G. (1993) Deformation characteristics of the Sheeprock and Canyon Range thrust sheets (Sevier orogenic belt) based on microstructural and strain studies. *Geological Society of America Cordilleran—Rocky Mountain Meeting Abstracts*, **25**, 153.
Wheeler, J. (1986) Average properties of ellipsoidal fabrics: implications for two- and three-dimensional methods of strain analysis. *Tectonophysics* **126**, 259–270.
Woodward, N. B., Gray, D. R. and Spears, D. B. (1986) Including strain data in balanced cross-sections. *Journal of Structural Geology* **8**, 313–324.

APPENDIX

Description of procedures for Strain analysis

(1) A square sampling grid is selected on the basis of preliminary fieldwork in the Sheeprock thrust sheet.

(2) Oriented quartzite samples are collected along the grid making sure that cataclasites from the tear faults and normal faults were not sampled and that three mutually perpendicular sections could be obtained from each sample. The orientation of bedding, cleavage or any planar structure at the sample site was also recorded.

(3) Three mutually perpendicular sections are cut from each quartzite sample and made chips for preparation of thin-sections. The positions of the chips on the cut surfaces were carefully marked.

(4) Colored photomicrographs were taken from each of the three thin-sections. In shooting the photomicrographs, I tried to ensure that the edges of the glass slide were parallel to the field of view so that the photomicrographs are oriented parallel to the glass slide and orientations of lines measured on the plane of the photomicrographs can be directly transferred to the sample face from which the slide was made.

(5) A black and white tracing of the quartz grains is prepared for each of the three mutually perpendicular thin sections for each sample (e.g. Fig. 5). The tracing was used to calculate the co-ordinates of the center and area of each grain in the tracing by using JAVA Image Analysis Software (Jandel Video Analysis Software, 65, Koch Road, Corte Madera, CA 94925, U.S.A.) installed on an IBM-PC with Video camera and PCVISION plus Frame Grabber (Imaging Technology Inc). First, I put the black and white tracing under the camera of the Image Analysis system and activated it. An image of the tracing was seen on the video monitor. I then moved the tracing around so that the edges of the tracing were parallel to the edges of the monitor and the orientation of the long axis of the calculated strain ellipses can be accurately recorded and transferred to the corresponding cut section on the quartzite sample. JAVA recognizes individual grains in the tracing as areas consisting of white pixels surrounded by grain boundaries consisting of black pixels. I also used the JAVA software to smoothen out the image and adjust the contrast between the grains and the grain boundaries in such a way that the least possible thickness of grain boundaries is obtained without disrupting the continuity of the grain boundaries (so that the grains do not join together and compromise the accuracy of the process). Once the image was satisfactorily adjusted, an 'intensity threshold' was set for grain counting to begin. At the end of grain-counting, JAVA determined the centroids and areas of individual grains and created an ASCII file containing the X and Y co-ordinates of the centroids and the areas of the along with a number of other parameters. The ASCII file needs to be edited so that only the X and Y co-ordinates of the centroids and the area of the grains are saved in the ASCII (.PRN) file created by JAVA.

(6) Data files are read into the program ANNGRAIN (McNaught, 1990), which calculates the two-dimensional strain ellipse using the modified normalized Fry Method. I recorded the axial ratio (R) and the orientation (θ) of the long axis of the calculated finite strain put out by ANNGRAIN. Thus, three finite strain ellipses, their axial ratios and long axes orientations, were obtained for the three mutually perpendicular sections from each quartzite sample.

(7) The strain ellipses determined for three mutually perpendicular sections must be now checked for strain compatibility. The strain compatibility test examines whether or not the three sectional strain

ellipses calculated for each sample lie on the surface of any real ellipsoid. If strain compatibility is satisfied, deformation occurred in a body without discontinuities or holes and the deformed body was coherent. I checked for strain compatibility using the '2D–3D Compatibility' program (DePaor, 1990). In most of the samples I examined, strain compatibility was satisfied by the sectional strain ellipses. A few were made compatible by adjusting the area stretch factor in the sectional strain ellipses as recommended by DePaor (1990).

(8) The strain ellipsoid at each sample location is calculated for each quartzite sample using the three sectional ellipses. To do this, I first oriented the quartzite sample in the laboratory with the help of the orientation mark made in the field and measured the attitude of the three planes on which the strain ellipses were computed. The strike lines and the dip directions for each plane were also sketched on to the corresponding rock surface. The long axes of the three strain ellipses were sketched on to the corresponding planes using the computed q values. I calculated the rakes (angle and direction) of the long axes of the three strain ellipsoids on the corresponding planes and then, using a stereonet, I calculated the attitude of the long axes of the three strain ellipses. Care must be taken when deciding on the rake directions of the long axes of the strain ellipses on planes which are overturned.

(9) The three-dimensional strain ellipsoid is calculated at each sample location by using the program 2D→3D which is distributed as part of the MacStrain 2.4 package written by K. Kanagawa at the University of Tokyo. This program determines strain ellipsoids from two-dimensional section data on any three sections that are not necessarily orthogonal. This program requires axial ratios and long-axis orientations of average marker ellipses on three sections with known orientations. The strain ellipsoid calculation in the program is based on Shimamoto and Ikeda (1976) and Wheeler's tensor algebraic method (Wheeler, 1986). Kanagawa's program also calculates a normalized final average ellipsoid using Milton's method (Milton, 1980) from data on three non-orthogonal sections which I have used as the representative finite strain ellipsoid at each sample location.